ELSEVIER

Chemical Engineering Science 61 (2006) 7199–7212

Chemical Engineering Science

www.elsevier.com/locate/ces

Flow patterns in the wake of a Taylor bubble rising through vertical columns of stagnant and flowing Newtonian liquids: An experimental study

S. Nogueira[a,b], M.L. Riethmuller[b], J.B.L.M. Campos[a], A.M.F.R. Pinto[a,*]

[a]*Centro de Estudos de Fenómenos de Transporte, Departamento de Eng. Química, Faculdade de Engenharia da Universidade do Porto, Rua Dr. Roberto Frias, 4200 - 465 Porto, Portugal*

[b]*von Kármán Institute for Fluid Dynamics, Chaussée de Waterloo, 72B-1640 Rhode Saint Genèse, Belgium*

Received 31 January 2006; received in revised form 1 August 2006; accepted 3 August 2006
Available online 8 August 2006

Abstract

The flow in the wake and near-wake regions of individual Taylor bubbles rising through stagnant and co-current vertical columns of Newtonian liquids was studied, employing simultaneously particle image velocimetry (PIV) and pulsed shadowgraphy techniques (PST). Experiments were made with water and aqueous glycerol solutions covering a wide range of viscosities (1×10^{-3} Pa s $< \mu <$ 1.5 Pa s), in an acrylic column of 32 mm ID.

Different wake structures (laminar, transitional and turbulent) are identified, in both stagnant and co-current flow conditions. In stagnant liquids, the wake flow pattern is only dependent on the dimensionless group N_f. The different types of wakes obtained are in accordance with the critical N_f numbers proposed in previous works. For co-current flow conditions, the flow patterns in the wake depend on the Reynolds number based on the relative (to the bubble) average velocity of the upward liquid flow, the laminar-transitional and transitional-turbulent limits being for the first time experimentally determined.

The wake flow patterns are quantified by means of instantaneous and average flow fields. Values for the wake length and wake volume are also presented and compare well with correlations found in literature. Study of the flow in the near-wake zone enabled determination of the distance needed to recover the undisturbed liquid velocity profile.

The detailed study of the flow in the wake and near-wake regions is an important contribution to better understanding the interaction and coalescence mechanisms between Taylor bubbles.

The data reported are relevant to the validation of numerical simulation codes in the vertical slug flow regime.

Keywords: Fluid mechanics; Multiphase flow; Slug flow; Bubble; Wakes; Particle image velocimetry (PIV)

1. Introduction

Slug flow is one of several gas–liquid flow regimes occurring inside pipes over a wide range of gas and liquid flow rates. In vertical flow, this pattern is characterized by long bullet-shaped bubbles, also called Taylor bubbles or gas slugs, which almost fill the pipe cross-section. Liquid moves around the bubbles and in the bulk between two successive gas slugs. The liquid moving around the bubble expands at the rear of the bubble, inducing a recirculating liquid wake.

Slug flow is found in many industrial applications, including hydrocarbon production in oil wells and their transportation in pipelines, nuclear reactors during emergency core cooling, power station steam boilers, transport and handling of cryogenic fluids, gas absorption units, heat exchangers, and air-lift reactors. A great amount of research has been devoted to the study of this two-phase flow regime (Dumitrescu, 1943; Moissis and Griffith, 1962; Nicklin et al., 1962; White and Beardmore, 1962; Brown, 1965; Wallis, 1969; Collins et al., 1978; Fernandes et al., 1983; Campos and Guedes de Carvalho, 1988a,b; Mao and Dukler, 1991; Barnea and Brauner, 1993; DeJesus et al., 1995; Pinto and Campos, 1996; Pinto et al., 1998, 2001; Bugg and Saad, 2002; van Hout et al., 2002; Viana et al., 2003; Funada et al., 2005; Nogueira et al., 2006; Taha and Cui, 2006,

* Corresponding author. Tel.: +351 22 508 1645; fax: +351 22 508 1449.
E-mail addresses: nogueira@fe.up.pt (S. Nogueira), riethmuller@vki.ac.be (M.L. Riethmuller), jmc@fe.up.pt (J.B.L.M. Campos), apinto@fe.up.pt (A.M.F.R. Pinto).

0009-2509/$ - see front matter © 2006 Elsevier Ltd. All rights reserved.
doi:10.1016/j.ces.2006.08.002

among others). An extensive review of this topic is given by Fabre and Liné (1992). Nonetheless, there remains much to investigate and understand of the flow pattern in the bubble wake region.

In a slugging column with gas and liquid flowing in co-current conditions, the flow field is extremely complex. A detailed study of the entire flow field around a Taylor bubble is a fundamental step towards a reliable hydrodynamic understanding and simulation of this two-phase flow pattern. Particularly the study of the wake region, because it plays an important role in several phenomena: (i) it is a region of intensive mass and heat transfer in all the processes where chemical reactions take place; (ii) it influences the interaction and coalescence between two consecutive Taylor bubbles.

The flow in the wake region has been studied by several authors. Using a Pitot tube, Moissis and Griffith (1962) measured the velocity profiles at various distances from the bubble rear and concluded that the dynamics of a Taylor bubble is disturbed by the flow pattern in the wake of the preceding bubble if they rise in close sequence. Maxworthy (1967) showed that separated liquid flow exists behind Taylor bubbles, by using a very simple visualization technique. Filla et al. (1979) studied the wakes of Taylor bubbles and concluded that they are turbulent if the bubbles rise through water in sufficiently large pipes.

Campos and Guedes de Carvalho (1988a) did a photographic study of the flow in the wake of individual Taylor bubbles rising in stagnant liquids. The authors identified three different flow patterns in the wake (laminar, transitional and turbulent). They stated that for sufficiently long bubbles (longer than $Z^* = [g\delta^2 2v + U_B]/2g$, where δ is the thickness of the stabilized annular liquid film flowing around the bubble and U_B stands for the bubble velocity) the type of flow pattern in the wake depends only on the inverse viscosity number, $N_f = (gD^3)^{1/2}/v$, where g is the acceleration due to gravity, D is the pipe diameter and v is the kinematic viscosity of the liquid.

1.1. Type I—closed axisymmetric wake: $N_f < 500$

A closed wake is observed to rise at the velocity of the bubble. The wake has an internal toroidal vortex, with the vortex ring lying in a plane perpendicular to the column axis. The bubble rear has the shape of an oblate sphere and rises steadily (no bottom oscillations are observed).

The dimensionless wake length, ℓ_w/D, increases with N_f, and Campos and Guedes de Carvalho (1988a) suggested the following linear relationship:

$$\frac{\ell_w}{D} = 0.30 + 1.22 \times 10^{-3} N_f, \quad 100 < N_f < 500. \tag{1}$$

An empirical correlation was also presented for the dimensionless wake volume, v_w/D:

$$\frac{v_w}{D} = 7.5 \times 10^{-4} N_f, \quad 100 < N_f < 500. \tag{2}$$

1.2. Type II—closed unaxisymmetric wake: $500 < N_f < 1500$

For this range of N_f a closed wake is still observed, but the rear surface of the bubble is now flat and the vortex ring shows a periodic undulation movement whose frequency increases with N_f. The liquid flowing below the wake is neither steady nor axisymmetric.

The size of the wake, ℓ_w/D, also increases with N_f, but the relation between these two parameters, Eq. (1), is only valid until $N_f = 800$.

1.3. Type III—opened wake with recirculatory flow: $N_f > 1500$

For $N_f > 1500$ the wake does not have a well-defined boundary. For values of N_f around and slightly above 1500, there are still some randomly located recirculating regions. For higher values of N_f, these zones disappear and the formation of turbulent eddies is observed. The action of these eddies is felt several diameters below the rear of the bubble. Lack of definition of the wake boundary makes it difficult to quantify the wake length by direct visual observation. However, Campos and Guedes de Carvalho (1988b) were able to calculate values of ℓ_w from mixing data in slugging columns by means of a simple model of axial transport of tracer. Values of ℓ_w calculated this way were shown to be in good agreement with values suggested by visual observation of the movement of small bubbles trailing behind each Taylor bubble.

For Taylor bubbles rising in co-current liquid conditions the flow is more complex and the determinant parameters are more difficult to identify, as pointed out by Pinto et al. (1998) in their attempt to describe the wake flow patterns.

The main difference between the flow patterns in the rear of Taylor bubbles rising in stagnant and co-current conditions is that, in the latter case, the emerging profile (from the wake region) develops in order to restore the main liquid profile (laminar or turbulent). Pinto et al. (1998) defined a dimensionless number, which should characterize the flow pattern in the wake:

$$Re_{V_L} = V_L D/v, \tag{3}$$

where V_L, the superficial liquid velocity relative to the bubble, is given by

$$V_L = U_B - U_L = (cU_L + U_\infty) - U_L, \tag{4}$$

where U_∞ is the bubble velocity in stagnant liquids, U_L is the mean upward liquid velocity in the tube and c a velocity coefficient equal to 1.2 when the liquid flow regime is turbulent and 2.0 when it is laminar.

Characterizing the wake flow pattern only by Re_{V_L}, Pinto et al. (1998) defined the following limits for the different flow regimes in the wakes:

Type I—closed and axisymmetric wake with internal recirculatory flow (laminar wake):

$$Re_{V_L} < 175. \tag{5}$$

Type II—closed and unaxisymmetric wake with internal recirculatory flow (transitional wake):

$$175 < Re_{V_L} < 525. \quad (6)$$

Type III—open and perfectly mixed wake (turbulent wake):

$$Re_{V_L} > 525. \quad (7)$$

These limits for the different flow patterns in the wake were not experimentally confirmed.

Pinto and Campos (1996) presented a systematic study of the coalescence of pairs of Taylor bubbles rising through a vertical column of a stagnant liquid for a wide range of liquid viscosities. The measurement technique was based on the signals of differential pressure transducers and the output was the minimum distance above which there is no coalescence, $\ell_{\min}$ (i.e., the minimum stable liquid length). They also determined the approach velocity of the trailing bubble as a function of the distance to the leading one. Three different relationships between $\ell_{\min}/D$ and the inverse viscosity number, N_f, according to the flow patterns in the wake, were found:

$$\frac{\ell_{\min}}{D} = 1.46 + 4.75 \times 10^{-3} N_f,$$
$$100 < N_f < 500 \quad \text{laminar wake}, \quad (8)$$

$$\frac{\ell_{\min}}{D} = 6.92 \times 10^{-1} + 7.90 \times 10^{-3} N_f,$$
$$500 < N_f < 1500 \quad \text{transitional wake}, \quad (9)$$

$$\frac{\ell_{\min}}{D} = 12.5, \quad N_f > 1500,$$
$$\text{turbulent wake}. \quad (10)$$

Recently, Nogueira et al. (2006) applied a non-intrusive technique combining particle image velocimetry (PIV) and pulsed shadowgraphy technique (PST) to characterize the flow in the nose region and in the annular film around the Taylor bubble.

In the present work, the same accurate technique was used to study the flow in the wake of individual Taylor bubbles rising in a 32 mm ID vertical tube. Different types of wake (laminar, transitional and turbulent) were identified, in both stagnant and co-current flow conditions. The wake flow patterns are described by means of instantaneous and average flow fields. Values for the wake length and volume are also presented. The study of the flow pattern in the near-wake region enabled the distance needed to recover the undisturbed liquid velocity profile to be determined. Experiments were performed for a wide range of liquid viscosities (1×10^{-3} Pa s $< \mu <$ 1.5 Pa s).

2. Experimental set-up and techniques

2.1. Facility

The present study was carried out in a set-up as sketched in Fig. 1, which is described in detail in Nogueira et al. (2003, 2006). The experiments were performed in a transparent acrylic column, 6 m long with a 0.032 m internal diameter. The test section was located near the top of the tube, to avoid entrance

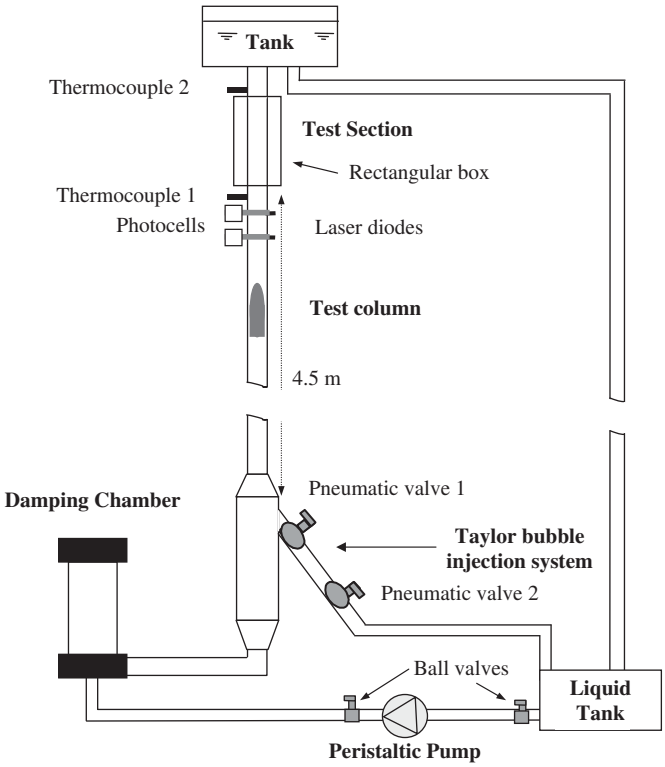

Fig. 1. Experimental set-up.

effects and to ensure fully-developed flow in the liquid ahead of the bubble (Moissis and Griffith, 1962). A transparent box with plane faces surrounded the test section (0.5 m × 0.12 m × 0.11 m), and was filled with the same liquid in study in order to minimize optical distortion.

Individual Taylor bubbles were generated and injected at the bottom of the column by manipulating valves 1 and 2 (Fig. 1). The volume of air/bubble used in these experiments ranged from 40×10^{-6} to 265×10^{-6} m^3 (NTP).

For the experiments in co-current flow conditions, the liquid flow rate was controlled by means of a peristaltic pump. In order to have a steady flow rate in the test tube, a damping chamber was placed between the pump outlet and the column inlet as suggested and used by Pinto et al. (1998). Some PIV measurements confirmed this steady state flow in the liquid and the absence of pulsating flow.

The system was thermally insulated and the temperature difference between top and bottom of the column was less than 0.3 °C, measured with thermocouples 1 and 2 (Fig. 1). The liquid viscosity was measured in a Brookfield rotating viscometer at working temperature, immediately after each set of experiments in order to minimize water absorption and evaporation. The range of viscosities covered was from 1×10^{-3} to 1.50 Pa s.

2.2. Measurement techniques

The Taylor bubble velocity was measured from the signals of two laser diodes 0.25 m apart, mounted perpendicularly to the tube and pointed at two corresponding photocells placed on

the opposite side of the column, as described in Nogueira et al. (2006).

The PIV/PST technique, fully described in Nogueira et al. (2003), consists of a board of light emitting diodes (LEDs) placed behind the test section, pulsing in synchronization with a laser source so that a CCD camera (PCO camera with a resolution of 1280 H × 1024 V and 4096 grey levels) was able to acquire a frame containing both the seeding PIV particles and the bubble shadow. The fluorescent seeding particles were a buoyant orange vinyl pigment (10 μm mean size) emitting light at 590 nm (a product from Lefranc and Bourgeois). Some sedimentation tests were made to confirm the buoyancy of the particles. A double-cavity pulsed Nd:Yag laser with a wavelength of 532 nm (pulse duration of 2.4 ns) with an adjustable pulse separation between each laser firing was used. The laser sheet had a thickness of about 1 mm in the test section. A red filter, opaque below 590 nm, was used to block the intense green laser reflections and to allow passage of the light emitted by the fluorescent particles and by the LEDs. For more details see Nogueira et al. (2003).

The synchronization between the laser, CCD camera and LEDs was made using a single signal generator, so that each frame of the camera simultaneously recorded a LED pulse and a laser pulse.

2.3. Data processing

The images recorded contained both the PST (bubble shape) and the PIV (flow field) information. The data processing was done separately as described by Nogueira et al. (2003).

The flow field in the liquid was obtained by processing the acquired images with the cross-correlation window-displacement-iterative-multigrid algorithm (WIDIM), developed by Scarano and Riethmuller (1999). In this work the initial image had 1280 (V) × 1024 (H) pixels and the initial window size was 64 × 32 pixels, according to the flow direction. Two refinements were performed to reach final interrogation windows of 16 × 8 pixels. An overlap of 50% refined the grid spacing to 8 × 4 pixels, which allowed a resolution of 0.342 mm × 0.171 mm ($0.01D \times 0.005D$) in the measurements in the wake and near-wake region. The time gap between the pulsing of the two laser cavities (pulse separation) was adjusted according to the measured velocities and varied from 120 to 2000 μs. Identification of spurious vectors was made, and vectors with signal-to-noise (SN) ratios less than 1.5 (around 4–6% of all processed vectors, for the whole set of conditions studied) were eliminated. Interpolated vectors from the adjacent neighbors replaced these spurious vectors. The average SN in a processed PIV image was around 10. Some erroneous vectors appeared inside the bubble, due to virtual particle images formed by refraction and reflection of the light emitted by the particles at the gas–liquid interface. Elimination of these vectors was possible since simultaneous PIV and PST allows determination of the exact position of the interface. The image procedure to obtain the shadow of the bubble was performed in several steps, as described in detail by Nogueira et al. (2003).

Tests made with known particle displacements showed a maximum uncertainty of 0.2 pixels on the windows displacement in the liquid velocity measurements. This corresponds to a maximum relative error of around 4% in the liquid velocity in the wake and near-wake region for all the solutions studied and PIV times chosen.

3. Results and discussion

The flow field in the wake and near-wake region of individual Taylor bubbles rising through stagnant (S) and co-current (CC) flowing liquids was obtained. The experimental conditions are listed in Table 1.

The measured values of the Taylor bubble velocity in stagnant conditions, U_B, are in very good agreement with those predicted by the empirical correlations of White and Beardmore (1962). For the experiments in co-current flow, the experimental values of U_B were compared successfully with Nicklin's predictions (Nicklin et al., 1962):

$$U_B = cU_L + \alpha\sqrt{gD} = cU_L + U_\infty, \tag{11}$$

where α is a parameter dependent on the viscous, interfacial and inertial forces (White and Beardmore, 1962).

In the present work all the experiments were performed with long Taylor bubbles in order to have a fully developed annular film (length greater than Z^*) flowing around the bubble, but not long enough as to allow development of rippling waves.

The wake flow patterns are described by means of instantaneous and average flow fields as well as by the corresponding streamlines. The origin of the axial coordinate z in all the following figures is at the Taylor bubble rear. The axial velocity component is positive, downwards. The origin of the radial coordinate is at the column axis. A positive radial velocity component represents liquid moving from the tube axis to the right (paper plane) and a negative one liquid moving from the tube axis to the left (paper plane).

Fig. 2 shows the shadow of the bottom of a Taylor bubble rising in a viscous stagnant solution, $N_f = 200$. A slightly concave depression at the bubble trailing edge is clearly seen. In the paper plane, this depression is covered by the 2D

Table 1
Experimental conditions

μ (Pa s)	ρ (kg/m^3)	U_L (m/s)	U_B (m/s)	N_f	Re_{VL}	S/CC
1.499	1262	0.000	0.120	15	–	S
0.205	1232	0.055	0.303	108	48	CC
0.199	1233	0.000	0.188	111	–	S
0.109	1222	0.000	0.197	200	–	S
0.043	1200	0.000	0.197	505	–	S
0.046	1202	0.014	0.226	470	178	CC
0.043	1200	0.074	0.364	496	257	CC
0.025	1183	0.000	0.197	844	–	S
0.015	1168	0.006	0.203	1360	476	CC
0.014	1170	0.000	0.197	1456	–	S
0.014	1169.7	0.080	0.358	1506	748	CC
0.002	1071	0.000	0.197	8078	–	S
0.001	1000	0.000	0.197	17 929	–	S

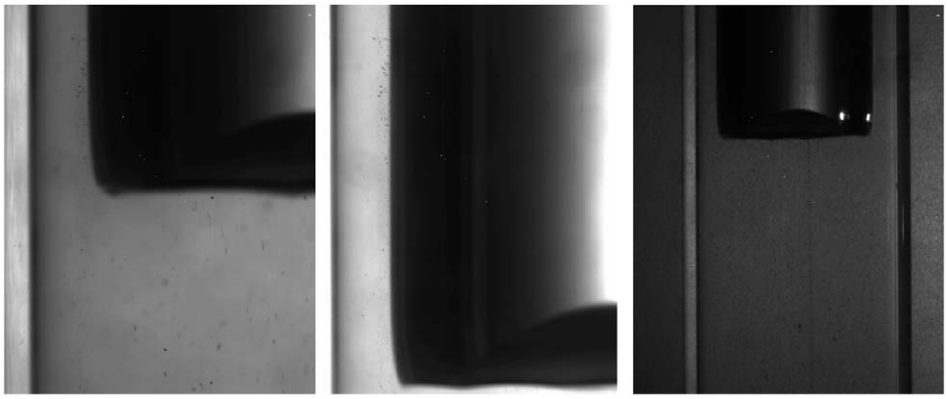

Fig. 2. Shadow of the bottom of isolated Taylor bubbles rising in a stagnant solution, $N_f = 200$.

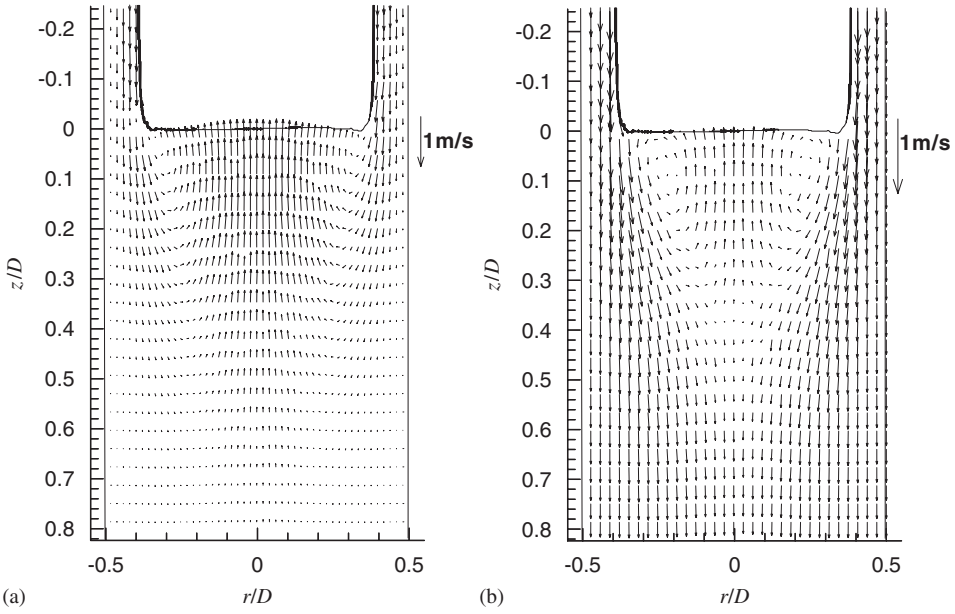

Fig. 3. Instantaneous velocity profiles at the rear of the Taylor bubble rising isolated in a stagnant aqueous glycerol solution, $N_f = 200$; (a) in a fixed frame of reference (FFR) and (b) in a moving frame of reference (MFR).

projection of the bubble surface and, consequently, the velocity field inside is hidden. Nevertheless, the instantaneous velocity fields obtained, such as those represented in Fig. 3, give useful information. The flow coming from the liquid film arrives at the bubble bottom and begins to decelerate in order to occupy the entire tube cross-section. Like the flow in a sudden expansion, the length needed to achieve total deceleration of the annular liquid film depends on the competition between the radial diffusion of momentum (inwards) and the axial convective transport of momentum (downwards). In most of the studied conditions (both with stagnant and co-current flowing liquids), a separated toroidal recirculation zone is established behind the rear of the bubble. Inside the wake the fluid undergoes an intense recirculation, with a mean upward velocity equal to the bubble velocity. To get an accurate flow characterization, the velocity vectors at each coordinate in the wake of 10 identical Taylor bubbles were averaged. The results are represented in Fig. 4 in a fixed frame of reference (FFR) and in a reference moving with the bubble (MFR). Fig. 5 shows the streamlines determined from the averaged flow field in a frame of reference attached to the bubble. The toroidal vortex is well identified, the symmetry is evident and the bottom of the wake, where the streamlines from the liquid film reattach, is well defined. The axial position of the vortex core is found to be around $z/D = 0.09$, while the radial position is around $r/D = 0.22$. This flow pattern is in accordance with the findings reported by Campos and Guedes de Carvalho (1988a) for this operating condition ($N_f = 200$).

The bubble wake can be further characterized by determining the wake length, ℓ_w, and the wake volume, v_w. To highlight the wake region, the boundary of the wake can be drawn by performing mass balances along the axial direction as described by Nogueira et al. (2003). Considering a frame of reference moving with the Taylor bubble, the downward liquid flow rate

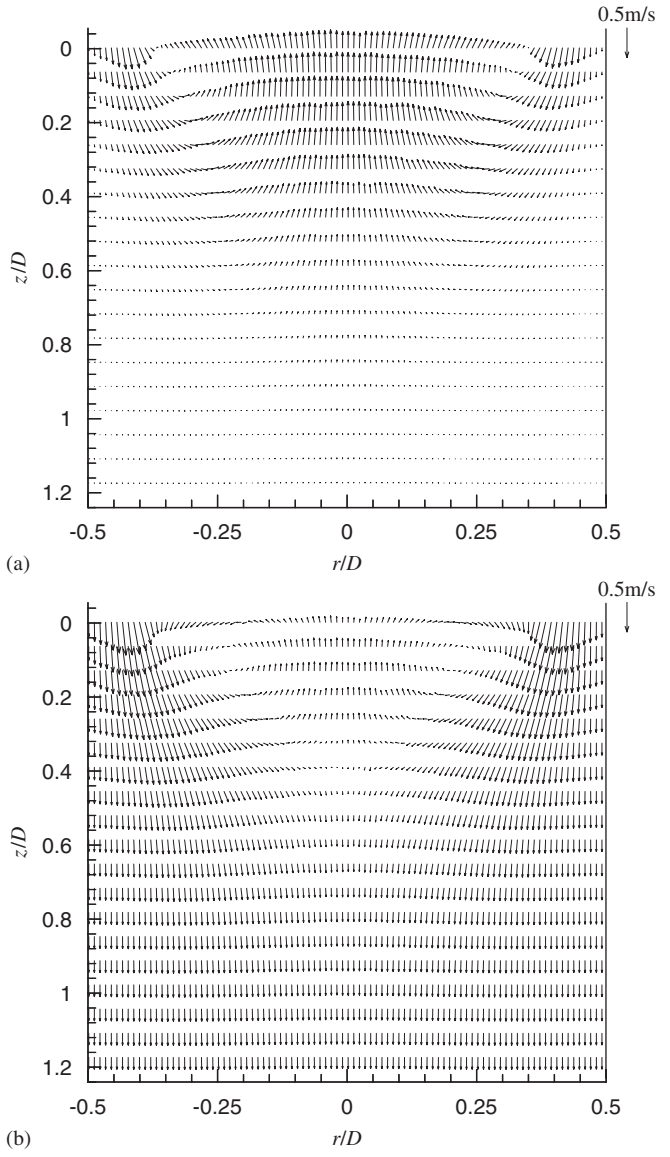

Fig. 4. Average flow field in the wake of a Taylor bubble rising in a solution, $N_f = 200$; (a) in an FFR and (b) in an MFR.

is equal to

$$Q_v = \pi(D/2)^2 U_B = \int_{r^*}^{(D/2)} (u_z + U_B) 2\pi r \, \mathrm{d}r, \tag{12}$$

where $u_z + U_B$ represents the liquid velocity relative to a frame moving with the bubble and r^* the radial position of the wake boundary. The integration of the experimental u_z data enables the determination of r^* along the wake region and the definition of the wake boundary as shown in Fig. 6. The wake length, ℓ_w, is defined as the distance between the trailing edge position at the axis of the column and the end of the wake (same radial position). The wake length measured in this way does not take into account the wake portion inside the concave bottom. The average of the obtained values of ℓ_w for 10 different Taylor bubbles is $\ell_w = 0.38D$.

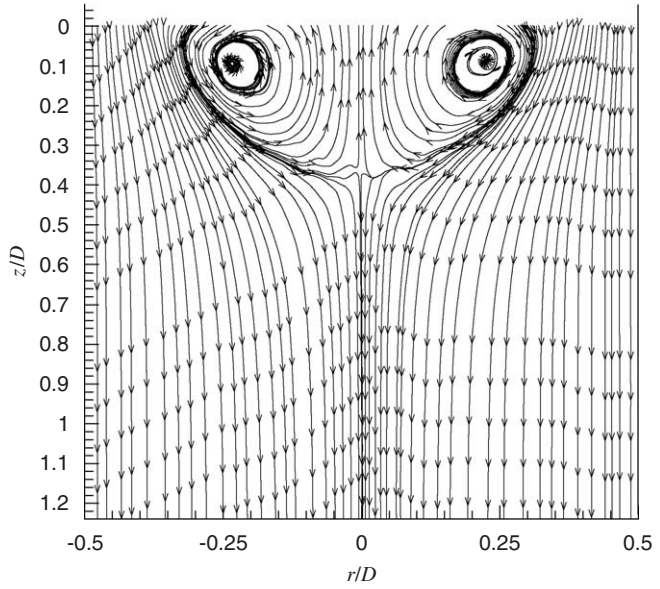

Fig. 5. Streamlines in the wake resulting from the averaging of the flow fields in the wake of ten different isolated Taylor bubbles rising in an aqueous glycerol solution, $N_f = 200$.

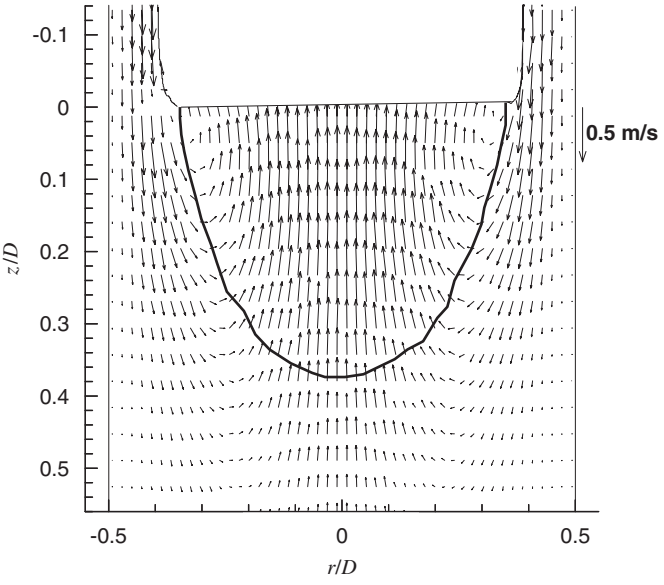

Fig. 6. Wake boundary determined by performing mass balances along the axial direction (Nogueira et al., 2003) superimposed on the velocity field represented in an FFR ($N_f = 200$).

The wake volume was determined revolving the boundary about the tube axis, i.e., assuming axisymmetric wakes. This procedure needs the wake boundary as an input. Once more, the calculated wake volume does not take into account the wake portion inside the concave bottom. For the present condition, the average wake volume is $v_w = 0.09D^3$.

The presence of the bubble is felt for some distance from the trailing edge. This distance, $\ell_{\min}$, was determined as follows. For seven equally distributed radial positions and different

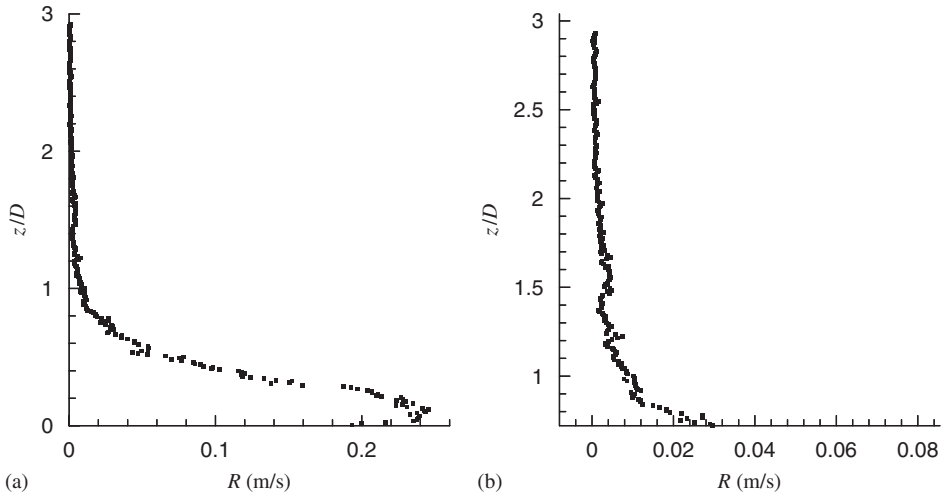

Fig. 7. Representation of the variable R along the axial distance from the bubble trailing edge for an isolated Taylor bubble rising in a stagnant aqueous glycerol solution, $N_f = 200$; (a) complete plot (b) zoom of the convergence region.

Table 2
Summary of the results obtained from the wake flow analysis

μ (Pa s)	N_f	Re_{VL}	S/CC	Flow pattern	ℓ_w/D	V_w/D^3	$\ell_{\min}/D$	$\ell_w/\ell_{\min} \times 100$ (%)
1.499	15	–	S	Laminar	–	–	0.8	–
0.205	–	48	CC	Laminar	0.25	0.037	0.7	36
0.199	111	–	S	Laminar	0.19	0.040	1.6	12
0.109	200	–	S	Laminar	0.38	0.091	2.4	16
0.043	505	–	S	Laminar	0.68	0.221	–	–
0.046	–	178	CC	Transition	0.74	0.248	–	–
0.043	–	257	CC	Transition	1.00	0.325	–	–
0.025	844	–	S	Transition	1.05	0.285	6.4	16
0.015	–	476	CC	Turbulent	–	–	–	–
0.014	1456	–	S	Transition	1.25	0.633	9.0	16
0.014	–	748	CC	Turbulent	–	–	–	–
0.002	8078	–	S	Turbulent	≈ 3	–	9.0	≈ 35
0.001	17 929	–	S	Turbulent	–	–	–	–

axial distances from the bubble bottom, values of the axial velocity component were extracted from the instantaneous velocity profiles. For each radial position, the square of the deviation between the local value of the axial velocity component and the value for the same radial position but far away from the bubble bottom was determined. The residual variable R, equal to the square root of the mean squared deviation (sum of the seven squared deviations divided by seven), was then computed and is represented versus the axial dimensionless distance from the bubble bottom, as illustrated in Fig. 7. The distance above which the flow is undisturbed behind the bubble is found to be around $z = 2.4D$ for the present condition.

Values for ℓ_w, v_w and $\ell_{\min}$ were determined for all the operating conditions studied and are accessible in Table 2.

Fig. 8 shows two consecutive shadow images of the rear of two Taylor bubbles rising in a less viscous aqueous glycerol solution, $N_f = 500$. For this condition the rear of the Taylor bubble is horizontal (perpendicular to the tube axis) in around 80% of the images taken and it is inclined, as depicted in the figure, for the other 20%.

Fig. 9 shows the streamlines drawn in the averaged flow field obtained from 13 Taylor bubbles with the trailing edges in a plane perpendicular to the column axis. The flow pattern in the wake is still an axisymmetric toroidal vortex. The other 20% show a slight non-symmetry in the wake and, consequently, a small inclination of the vortex ring.

The axial position of the vortex core is found to be around $z = 0.19D$, while the radial position is around $r = 0.26D$.

Individual Taylor bubbles rising in a less viscous stagnant solution, N_f=844, show unstable rears, with high frequency 3D oscillations of the trailing edge around the column axis. Vortex shedding is observed; however, its frequency and dependence on Reynolds number should be obtained in a more detailed study. Since PIV measurements were performed in the central vertical plane of the column and the shadowgraphy only gives a 2D projection of the bubble shape, it was impossible to describe the total flow features from instantaneous images. Due to the high frequency oscillations there is a lot of liquid crossing the measuring plane and so, some of the vectors represented are no more than projections in this plane. Therefore, the most

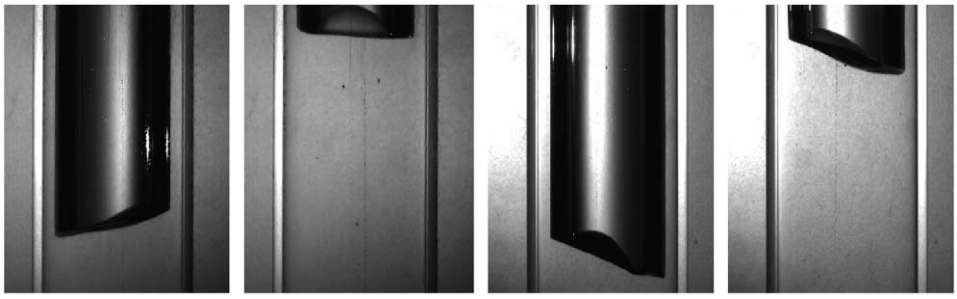

Fig. 8. Shadows of the rear of different isolated Taylor bubbles rising in a stagnant aqueous glycerol solution, $N_f = 505$.

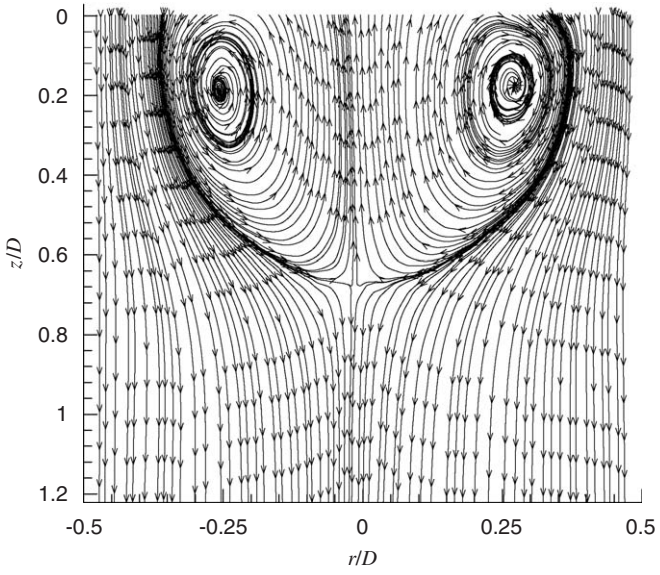

Fig. 9. Streamlines in the wake resulting from the averaging of the flow fields in the wake of thirteen different isolated Taylor bubbles rising in a stagnant aqueous glycerol solution, $N_f = 505$.

representative picture is the one based on an average from a significant number of images. Fig. 10 shows an average flow field (from 20 bubbles × 4 images from each bubble) in the wake of Taylor bubbles for this operating condition. In Fig. 11, the "streamlines" through all the vectors of this 2D flow field are represented.

From the previous figures, it cannot be concluded that the wake is completely closed. The two main recirculation regions (in the paper plane) are still observed, but it seems that one, i.e., almost one half of the wake, is in a shedding process. The flow pattern represented corresponds to a transitional wake, in agreement with the results presented by Campos and Guedes de Carvalho (1988a) for this condition.

A less viscous aqueous glycerol solution, $N_f = 8078$, was also studied. Fig. 12 shows four consecutive PIV images taken behind a Taylor bubble rising through this solution. The rear of the Taylor bubble is very unstable, presenting high amplitude and high frequency 3D movements. The presence of several small bubbles attached to the bottom of the Taylor bubble or rising inside the wake is also evident. This behavior was also reported previously by Campos and Guedes de Carvalho (1988a). The presence of these small bubbles leads to reflections of light and other optical problems, resulting in a poor SN ratio in the processed images. The small bubbles are still present at large distances from the bubble trailing edge, and in some way influence the liquid flow reattachment.

The instantaneous flow field in the wake of the Taylor bubble shown in Fig. 12 is represented in Fig. 13 in an MFR. The wake does not have a well-defined boundary and the flow pattern is extremely complex. The presence of some small recirculation zones can still be detected. Some liquid is rising upwards, following the bubble. The flow in the wake is turbulent, as reported by Campos and Guedes de Carvalho (1988a) for this operating condition.

The flow pattern in the wake of Taylor bubbles rising through co-current flowing liquids was also studied. For a given solution, the upward velocity of the liquid induces higher Taylor bubble velocities and, consequently, greater downward velocities in the liquid film flowing around them. The thickness of the stabilized film also increases. At the bubble rear, the film expands but at the same time it "merges" with the upward flowing liquid. After a certain distance from the bubble rear, the overall flow is upwards with a well-developed profile (parabolic if the flow in the main liquid is laminar). According to this simplified interpretation, the flow field in the flowing liquid is expected to have significant influence on the values of $\ell_{\min}$ and on the characteristics of the wake. This flow pattern description is supported by Fig. 14(a), representing the streamlines in the wake of a Taylor bubble rising in a co-current flowing liquid ($U_L = 0.014\,\mathrm{m/s}$ and $Re_{V_L} = 178$). The flow below the Taylor bubble was obtained from two consecutive PIV images since a single one was not able to capture the whole flow field. Due to the velocity of the Taylor bubble, a portion of the flow ($0.07D$) is lost and cannot be shown. There is a slight asymmetry in the wake flow. The core is at $z = 0.13D$ and $r \sim 0.27D$. The wake length is somewhat longer than the wake length of an identical bubble rising in the same solution when it is stagnant. Fig. 14(b) presents an instantaneous velocity field between $z = 0.3D$ and $1.1D$ and shows the redevelopment of the parabolic profile.

All the results obtained in the study of the wake flow pattern are summarized in Table 2. Three different types of wakes (laminar, transitional and turbulent) were identified, in both stagnant and co-current flow conditions.

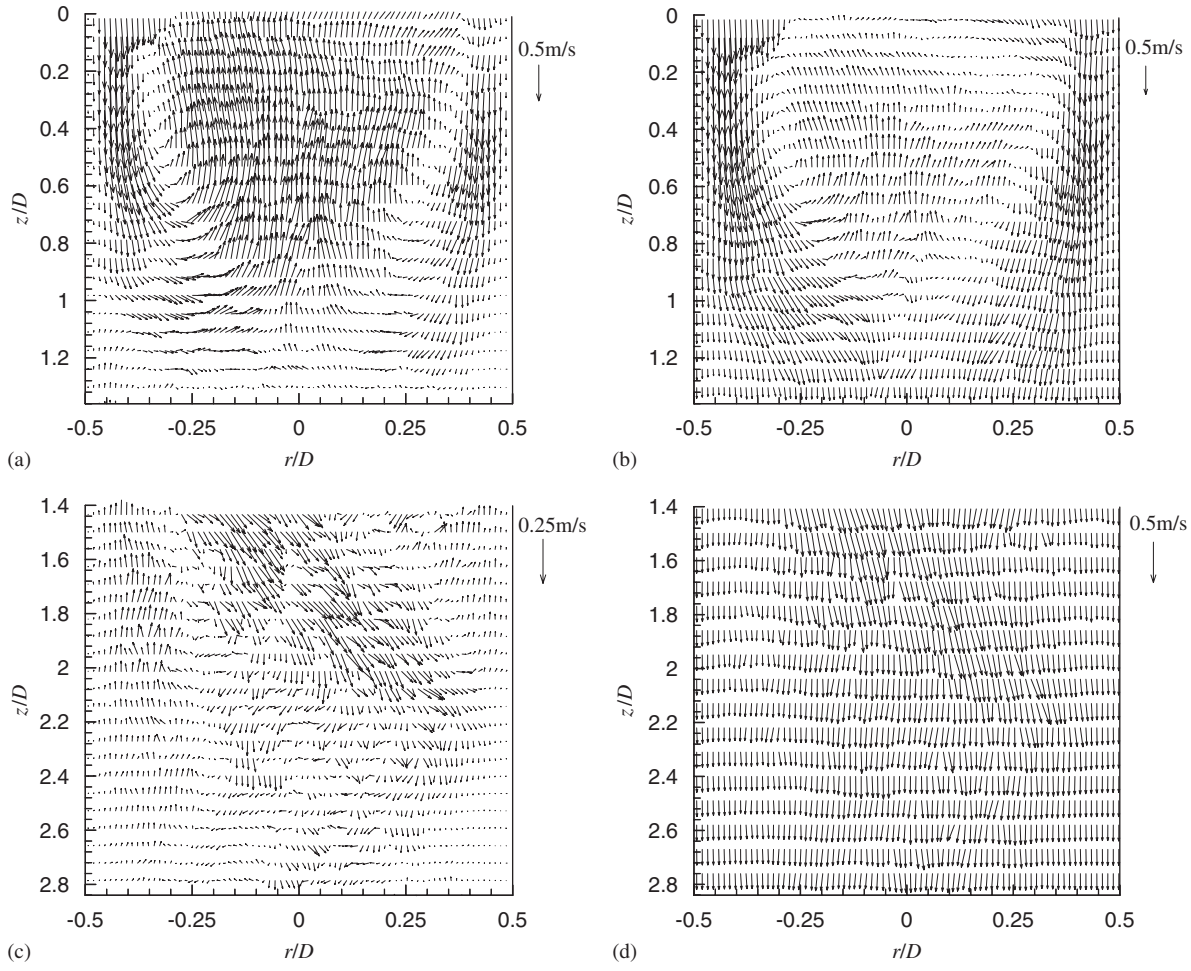

Fig. 10. Average flow field behind the wake of Taylor bubbles rising in an aqueous glycerol solution, $N_f = 844$, from the axial position $z/D = 0$ to around $z/D = 2.8$, (a), (c) in an FFR and (b), (d) in an MFR.

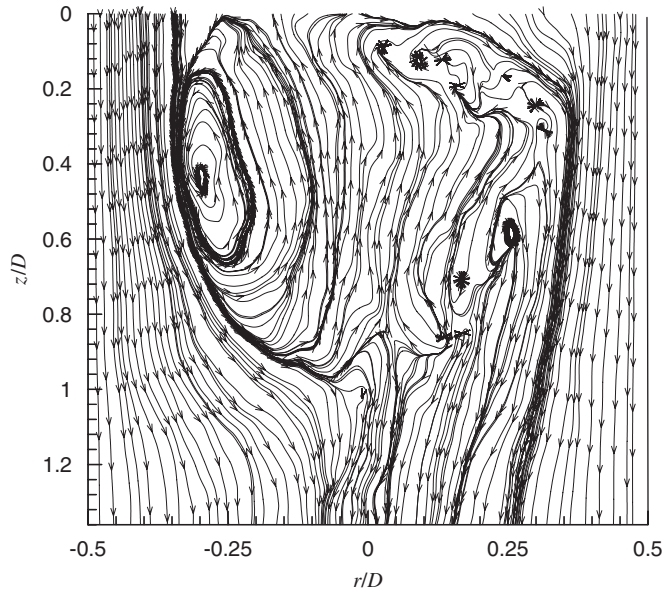

Fig. 11. Trajectories of the PIV particles in the wake resulting from the averaging of the flow fields of seven different Taylor bubbles rising in an aqueous glycerol solution, $N_f = 844$.

In stagnant conditions the wake flow pattern depends only on the dimensionless number, N_f, as proposed by Campos and Guedes de Carvalho (1988a). The N_f values referred to by those authors for the transition of regimes were also observed. For co-current flow conditions the three wake flow patterns depend on Re_{V_L} and the transitional Re_{V_L} values, proposed by Pinto et al. (1998), Eqs. (5)–(7), were experimentally confirmed for the first time.

In Fig. 15(a) the experimental values of the dimensionless wake length determined in this work for stagnant conditions are compared with the predictions of Campos and Guedes de Carvalho (1988a). The values reported are lower than the predictions (Eq. (1)). A plausible reason for this discrepancy is the experimental techniques used. Campos and Guedes de Carvalho (1988a) based their measurements on the visualization of colored dye which could diffuse even for laminar wakes, thereby giving longer wakes in the analysis. In the present work the wake lengths were taken from the measured velocity field in the wake and near-wake regions. As already mentioned, the discrepancy could also be due to the definition of the trailing edge origin, $(z/D = 0)$, ignoring or considering the portion of the wake inside the concave region at the bubble rear. In

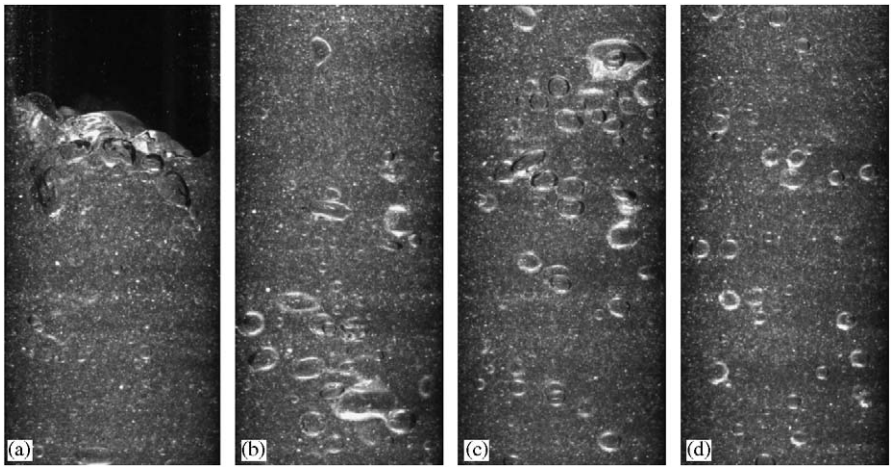

Fig. 12. Four consecutive PIV images behind a Taylor bubble rising isolated in an aqueous glycerol solution, $N_f = 8078$. (a) $-0.8 < z/D < 1.4$, (b) $0.7 < z/D < 2.9$, (c) $2.2 < z/D < 4.4$, (d) $3.7 < z/D < 5.9$.

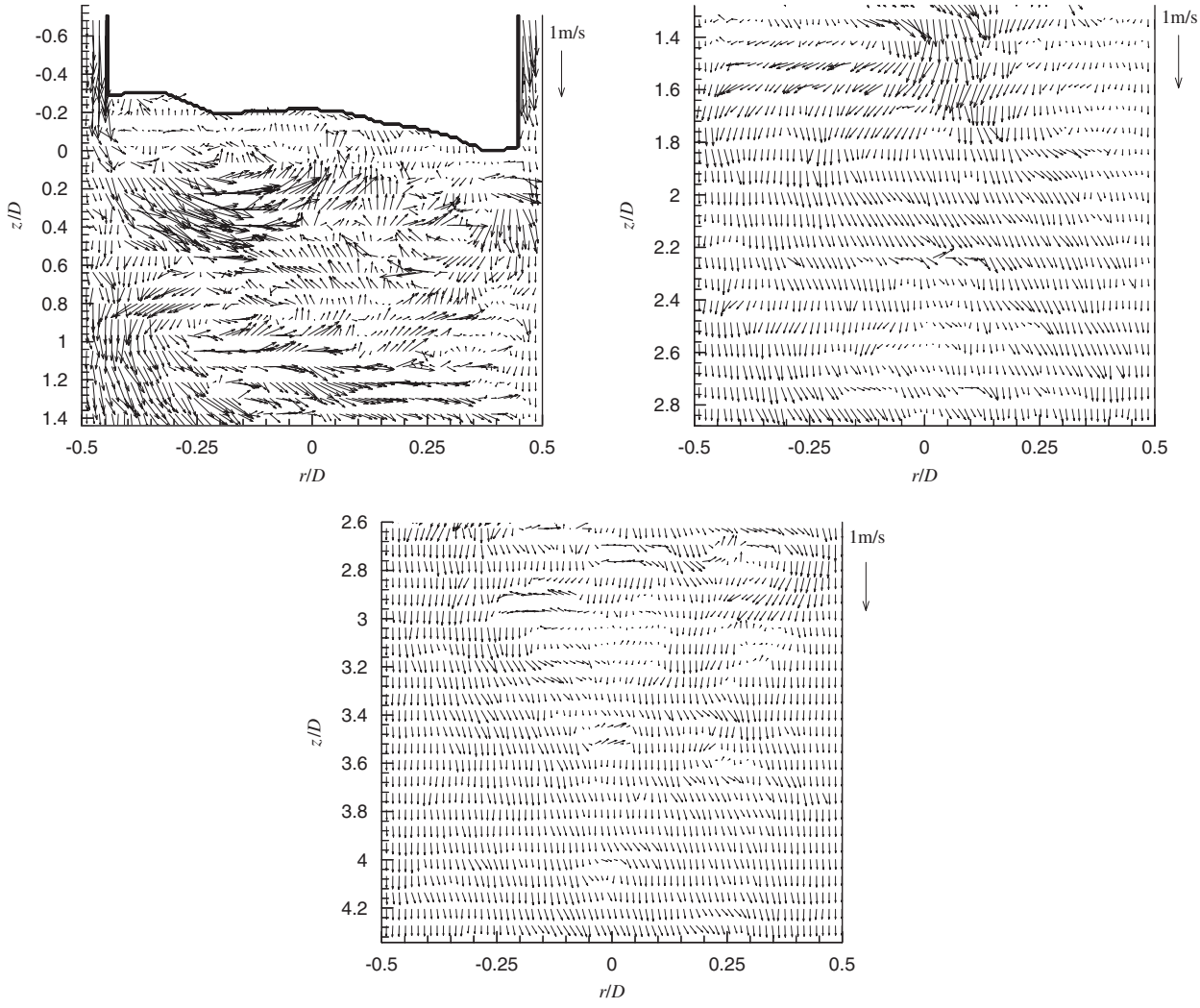

Fig. 13. Instantaneous flow fields (MFR) behind an isolated Taylor bubble rising in an aqueous glycerol solution $N_f = 8078$, for different axial positions.

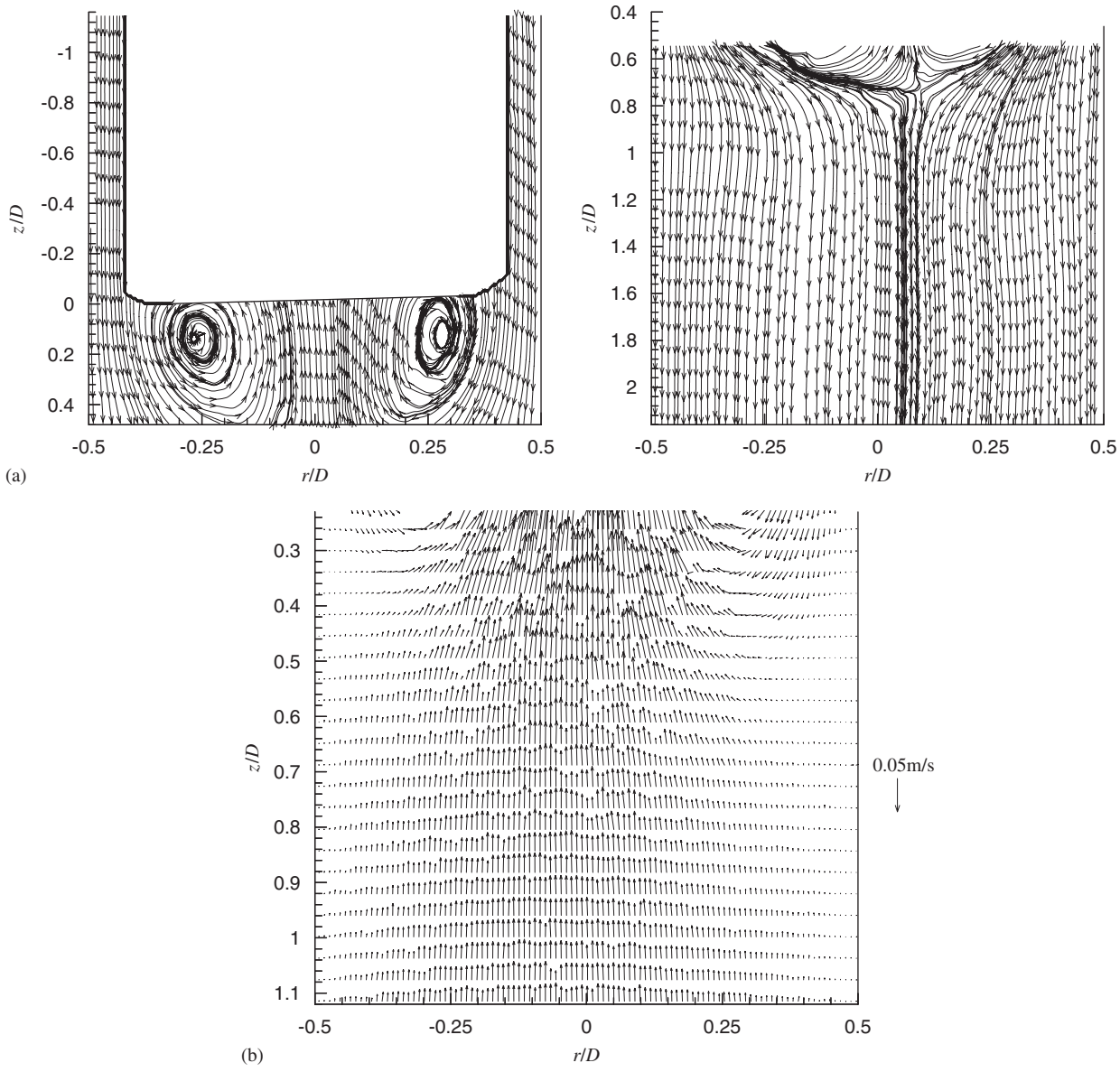

Fig. 14. (a) Streamlines in the wake of a Taylor bubble rising in a co-current flowing liquid ($U_L = 0.014$ m/s and $Re_{V_L} = 178$), (a) $0 < z/D < 0.46$, (b) $0.53 < z/D < 2.8$. (b) Zoom of the instantaneous flow field in the wake of a Taylor bubble rising in a co-current flowing liquid ($U_L = 0.014$ m/s and $Re_{V_L} = 178$) for $0.3 < z/D < 1.1$.

Fig. 15(a) some numerical results from the recent work of Taha and Cui (2006), also plotted for comparison, show a reasonable agreement with predictions from Eq. (1).

Fig. 15(b) shows the comparison between the experimental wake volumes, v_w/D, and the predictions from Eq. (2). The correlation also overestimates the wake volume and here the discrepancy increases with N_f.

In Figs. 16(a) and (b), the values obtained for dimensionless wake length and volume are plotted against Re_{V_L} for the co-current experiments. Both parameters seem to increase linearly with the dimensionless number Re_{V_L}. These are the first results, as far as we know, referred for the wake characterization in co-current flow. Additional conditions are needed to extend the range of operating conditions.

The study of the flow beyond the bubble wake enabled the determination of the minimum stable length between bubbles ($\ell_{\min}$), i.e., the distance needed to recover the undisturbed velocity profile. The values of $\ell_{\min}$ obtained in stagnant liquids for the three types of wakes (Table 2) are plotted in Fig. 17 versus N_f, together with the predictions of Pinto and Campos (1996). The experimental values are in accordance with the predictions except for the turbulent flow pattern, where the obtained constant value is 25% lower.

According to the data obtained, the length occupied by the wake is approximately 16% of $\ell_{\min}$ in both laminar and transition wakes (Table 2). Pinto and Campos (1996) found a value corresponding to 24% of the minimum stable length, whatever the flow pattern was.

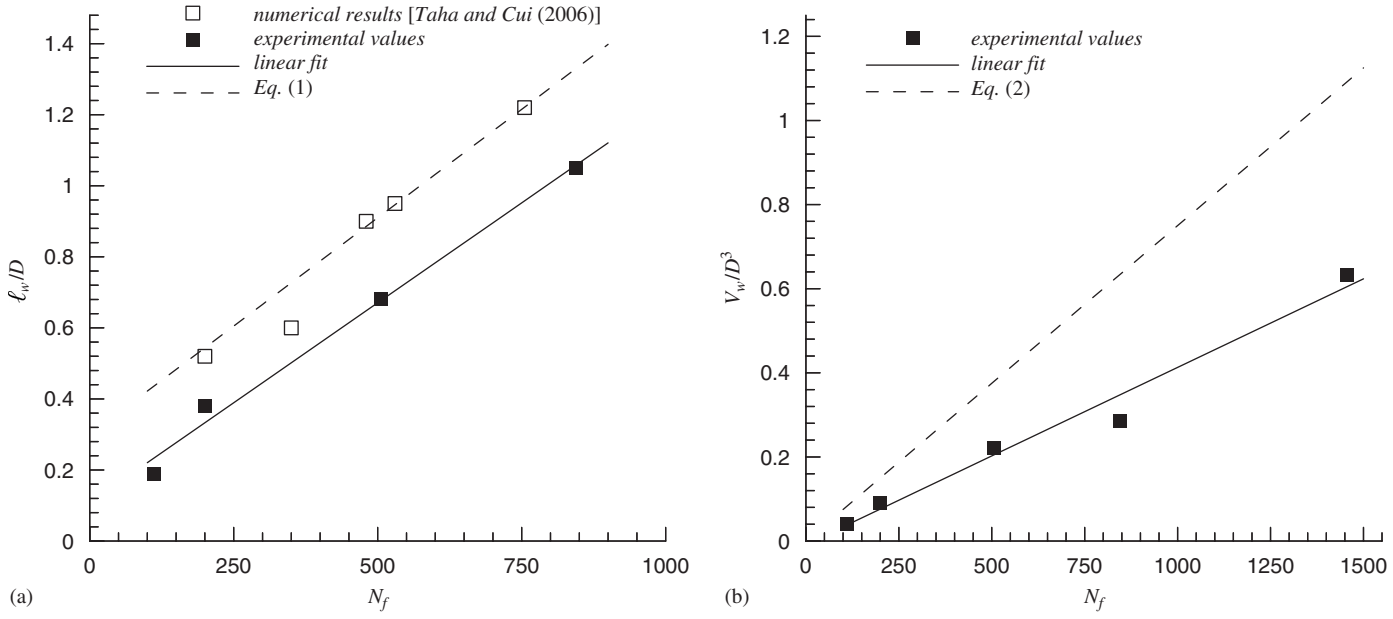

Fig. 15. (a) Dimensionless wake length versus N_f, for stagnant conditions (laminar and transitional wakes); comparison with Eq. (1) (Campos and Guedes de Carvalho, 1988a). (b) Dimensionless wake volume versus N_f, for stagnant conditions (laminar and transitional wakes); comparison with Eq. (2) (Campos and Guedes de Carvalho, 1988a).

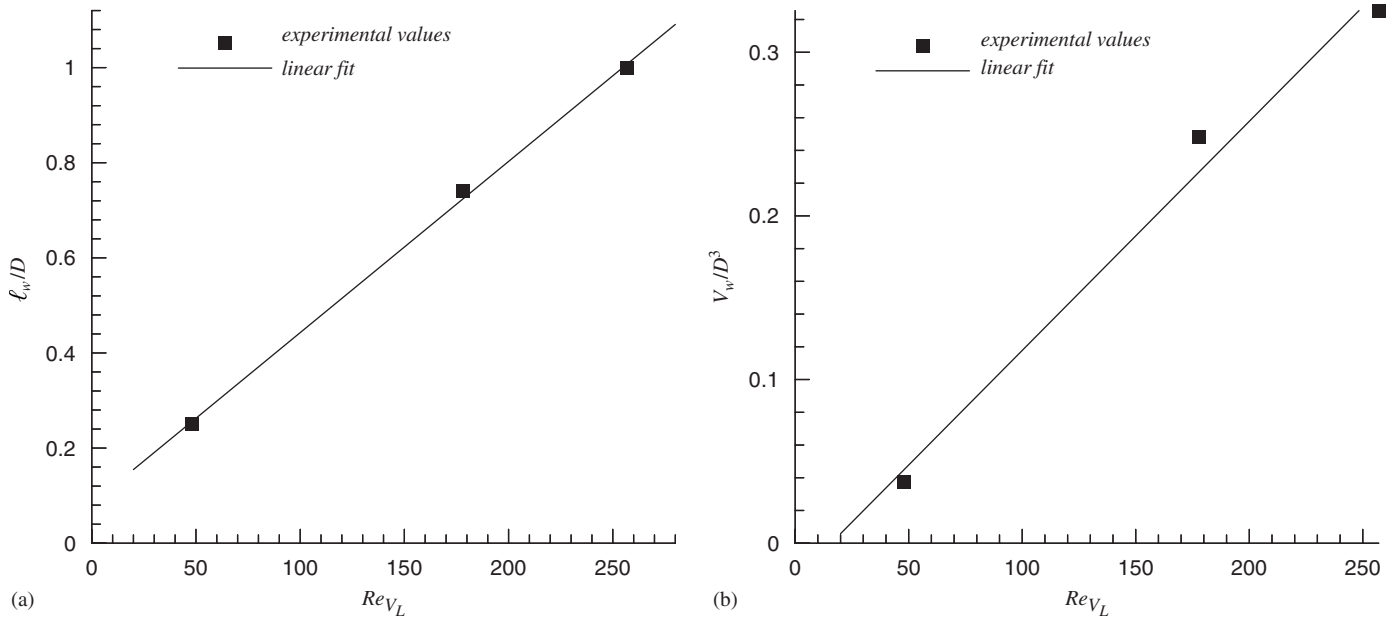

Fig. 16. (a) Dimensionless wake length versus Re_{V_L}, for co-current conditions. Linear fit: $\ell_W/D = 3.60 \times 10^{-3} Re_{V_L} + 0.083$ for laminar and transitional wakes. (b) Dimensionless wake volume versus Re_{V_L}, for co-current conditions. Linear fit, $v_W/D = 1.40 \times 10^{-3} Re_{V_L} - 0.022$, for laminar and transitional wakes.

The values of $\ell_{\min}$ obtained for low values of Re_{V_L} are lower than in stagnant conditions (identical liquid solution). This means that the "interaction" between the axial convective momentum in the liquid film (downwards) and the axial convective momentum in the flowing liquid (upwards) results in a shorter distance to the reestablishment of the undisturbed liquid flow pattern. These findings are in accordance with the work of Pinto et al. (1998).

4. Conclusions

Different type of wakes (laminar, transition and turbulent) at the rear of individual Taylor bubbles rising through Newtonian fluids were identified and characterized in both stagnant and co-current flow conditions. The wake flow patterns were analyzed by means of instantaneous and average flow fields.

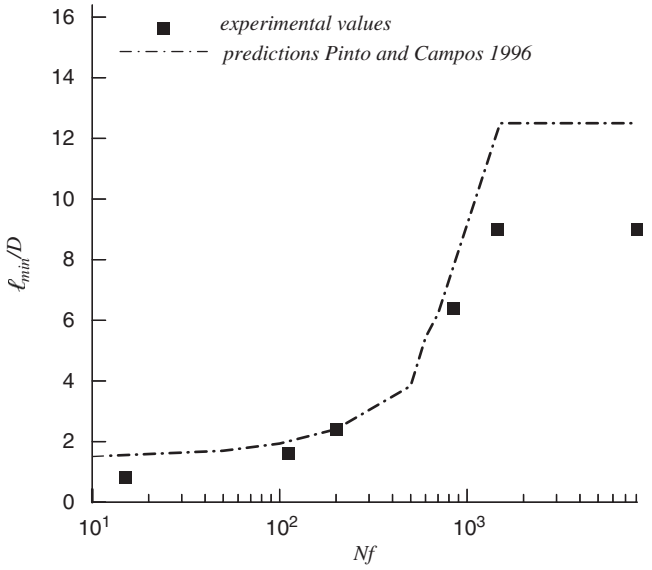

Fig. 17. Dimensionless minimum stable length, $\ell_{\min}/D$, versus N_f, for stagnant conditions; comparison with correlations of Pinto et al. (1996).

In stagnant conditions, the wake flow pattern depends only on the dimensionless number, N_f, as proposed by Campos and Guedes de Carvalho (1988a). The different types of wake flow patterns in the present work were obtained in accordance with the critical values of N_f number provided by these authors.

In co-current flow conditions the several flow patterns were experimentally obtained for the first time. The transition of the regimes was observed to be in accordance with the critical values of Re_{V_L} proposed by Pinto et al. (1998).

The dimensionless wake length and volume (for the laminar and transition cases) showed a linear increase with N_f (for stagnant conditions) and with Re_{V_L} (for co-current conditions). The study of the flow in the near-wake region enabled $\ell_{\min}$, the distance needed to recover the undisturbed velocity profile, to be determined.

In co-current conditions, the portion of $\ell_{\min}$ occupied by the wake is much more significant than in stagnant conditions, suggesting that the reestablishment of the original liquid flow pattern occurs in a shorter distance. These findings are in accordance with the work of Pinto et al. (1998).

This detailed study on the flow in the wake and near-wake region is an important contribution to the understanding of the coalescence mechanism. The results reported in this work for the flow around the Taylor bubble are relevant for the validation of numerical codes in slug flow.

Notation

Acronyms

CC	co-current conditions (Tables 1 and 2)
FFR	fixed frame of reference
MFR	moving frame of reference
NTP	normal temperature and pressure conditions (20 °C and 1 atm)
S	stagnant conditions (Tables 1 and 2)
SN	signal-to-noise ratio

Roman letters

c	velocity coefficient (Eqs. (3) and (4))
D	internal column diameter, m
g	acceleration due to gravity, m/s^2
H	number of pixels in the horizontal direction
$\ell_{\min}$	minimum distance between bubbles above which there is no coalescence, m
ℓ_w	wake length, m
Q_v	liquid volumetric flow rate, m^3/s
r	radial position, m
r^*	radial position of the wake boundary, m
R	mean residual variable, m (Fig. 7)
u_r	radial component of the velocity, m/s
u_z	axial component of the velocity, m/s
U_B	Taylor bubble velocity, m/s
U_L	mean superficial liquid velocity, m/s
U_∞	velocity of an individual bubble rising in a stagnant liquid, m/s
v_w	wake volume, m^3
V	number of pixels in the vertical direction
V_L	superficial liquid velocity relative to the bubble, m/s
z	distance from the Taylor bubble rear, m
Z^*	film developing length, m

Dimensionless groups

N_f	dimensionless parameter $\left(=\frac{(gD^3)^{1/2}}{\nu}\right)$
Re_{V_L}	Reynolds number based on the superficial liquid velocity relative to the bubble $\left(=\frac{V_L D}{\nu}\right)$

Greek letters

α	parameter (Eq. (4)), m
δ	liquid film thickness, m
μ	liquid dynamic viscosity, Pa s
ν	liquid kinematic viscosity, m^2/s
ρ	liquid density, kg/m^3

Acknowledgments

The partial support of "Fundação para a Ciência e Tecnologia—Portugal" through project POCTI/EQU/33761/1999 is gratefully acknowledged. POCTI (FEDER) also supported this work via CEFT.

References

Barnea, D., Brauner, N., 1993. A model for slug length distribution in gas–liquid slug flow. International Journal of Multiphase Flow 19, 829–838.

Brown, R.A.S., 1965. The mechanism of large bubbles in tubes. I. Bubble velocities in stagnant liquids. Canadian Journal of Chemical Engineering 43, 217–223.

Bugg, J., Saad, G.A., 2002. The velocity field around a Taylor bubble rising in a stagnant viscous fluid: numerical and experimental results. International Journal of Multiphase Flow 28, 791–803.

Campos, J.B.L.M., Guedes de Carvalho, J.R.F., 1988a. An experimental study of the wake of gas slugs rising in liquids. Journal of Fluid Mechanics 196, 27–37.

Campos, J.B.L.M., Guedes de Carvalho, J.R.F., 1988b. Mixing induced by slugs rising in narrow columns of water. Chemical Engineering Science 43, 1569–1582.

Collins, R., De Moraes, F.F., Davidson, J.F., Harrison, D., 1978. The motion of a large gas bubble rising through liquid flowing in a tube. Journal of Fluid Mechanics 89, 497–514.

DeJesus, J.D., Ahmad, W., Kawaji, M., 1995. Experimental study of flow structure in vertical slug flow. Advances in Multiphase Flow 31, 105–118.

Dumitrescu, D.T., 1943. Strömung an einer Luftblase im Senkrechten Rohr. Zeitschrift fur Angewandte Mathematik and Mechanik 23, 139–149.

Fabre, J., Liné, A., 1992. Modeling of two-phase slug flow. Annual Review of Fluid Mechanics 24, 21–46.

Fernandes, R.C., Semiat, R., Dukler, A.E., 1983. A Hydrodynamic model for gas-liquid slug flow in vertical tubes. A.I.Ch.E. Journal 29, 981.

Filla, M., Donsi, G., Crescitelli, S., 1979. Techniche sperimentali per lo studio della scia di bolle. ICP-Rivista Industria Chimica VII (10) (ottobre).

Funada, T., Joseph, D., Maehara, T., Yamashita, S., 2005. Ellipsoidal model of the rise of a Taylor bubble in a round tube. International Journal of Multiphase Flow 31, 473–491.

van Hout, R.V., Gulitsky, A., Barnea, D., Shemer, L., 2002. Experimental investigation of the velocity field induced by a Taylor bubble in stagnant water. International Journal of Multiphase Flow 29, 579–596.

Mao, Z.-S., Dukler, A., 1991. The motion of Taylor bubbles in vertical tubes. II—experimental data and simulations for laminar and turbulent flow. Chemical Engineering Science 46, 2055–2064.

Maxworthy, T., 1967. A note on the existence of wakes behind large rising bubbles. Journal of Fluid Mechanics 27, 367–368.

Moissis, R., Griffith, P., 1962. Entrance effects in a two-phase slug flow. Journal of Heat Transfer 84, 29–39.

Nicklin, D.J., Wilkes, J.O., Davidson, J.F., 1962. Two-phase flow in vertical tubes. Transactions of the Institution of Chemical Engineers and Chemical Engineer, 4061–4068.

Nogueira, S., Sousa, R.G., Pinto, A.M.F.R., Riethmuller, M.L., Campos, J.B.L.M., 2003. Simultaneous PIV and pulsed shadow technique in slug flow: a solution for optical problems. Experiments in Fluids 35, 598–609.

Nogueira, S., Riethmuller, M.L., Campos, J.B.L.M., Pinto, A.M.F.R., 2006. Flow in the nose region and annular film around a Taylor bubble rising through vertical columns of stagnant and flowing Newtonian liquids. Chemical Engineering Science 61, 845–857.

Pinto, A.M.F.R., Campos, J.B.L.M., 1996. Coalescence of two gas slugs rising in a vertical column of liquid. Chemical Engineering Science 51, 45–54.

Pinto, A.M.F.R., Coelho Pinheiro, M.N., Campos, J.B.L.M., 1998. Coalescence of two gas slugs rising in a co-current flowing liquid in vertical tubes. Chemical Engineering Science 53, 2973–2983.

Pinto, A.M.F.R., Coelho Pinheiro, M.N., Campos, J.B.L.M., 2001. On the interaction of Taylor bubbles rising in two-phase co-current slug flow in vertical columns: turbulent wakes. Experiments in Fluids 31, 643–652.

Scarano, F., Riethmuller, M.L., 1999. Iterative multigrid approach in PIV image processing with discrete window offset. Experiments in Fluids 26, 513–523.

Taha, T., Cui, Z.F., 2006. CFD modeling of slug flow in vertical tubes. Chemical Engineering Science 61, 676–687.

Viana, F., Pardo, R., Yanez, R., Trollero, R., Joseph, D., 2003. Universal correlation for the rise velocity of long gas bubbles in round pipes. Journal of Fluid Mechanics 494, 379–398.

Wallis, G.B., 1969. One-Dimensional Two-Phase Flow. McGraw Hill, New York.

White, E.T., Beardmore, R.H., 1962. The velocity of rise of single cylindrical air bubbles through liquids contained in vertical tubes. Chemical Engineering Science 17, 351–361.